Lecture 4: Resonance and Solutions to the LTE

Myrl Hendershott and Chris Garrett

1 Introduction

Myrl Hendershott concluded the last lecture by discussing the normal modes of the ocean, i.e. the free wave solutions of the Laplace Tidal equations. Today, we will review these concepts and extend them to so solve for specific instances of gravity and Rossby modes in simple basins. We will then discuss the computation work of Platzman [1] on the normal modes in the oceans and describe resonance in the seas.

The second half of the lecture was given by Chris Garrett and served as an introduction to his lectures during the second week. He motivates the study of tides by discussing them in the contexts of observations at several different geographical locations. He then adds to Myrl Hendershott's discussion on resonance with observations and some inferences about friction.

2 Review of Normal Modes

In plane coordinates, the Laplace Tidal equations (LTE) are given by

$$\begin{aligned} u_t - fv &= -g\zeta_x, && (1)\\ v_t + fu &= -g\zeta_y, && (2)\\ \zeta_t + D\left(u_x + v_y\right) &= 0, && (3) \end{aligned}$$

where $f = f_0 + \beta y$ and $D = D_n$, where D_n is a constant determined by an appropriate eigenvalue problem discussed in the previous lecture. To find free solutions of the LTE we look for harmonic solutions, i.e. solutions with time dependence proportional to $e^{-i\sigma t}$ which can be seen as transforming the time derivatives by

$$\frac{\partial}{\partial t} \rightarrow -i\sigma. \tag{4}$$

That is, the LTE become

$$\begin{aligned} -i\sigma u - fv &= -g\zeta_x, && (5)\\ -i\sigma v + fu &= -g\zeta_y, && (6)\\ -i\sigma\zeta + D\left(u_x + v_y\right) &= 0. && (7) \end{aligned}$$

Solving for u and ζ in terms of v, the LTE can be reduced into a single second order partial differential equation for v. We find that

$$\nabla^2 v + i\frac{\beta}{\sigma}v_x + \frac{\sigma^2 - f^2}{gD}v = 0. \tag{8}$$

If we seek plane wave solutions for v i.e. $v = e^{-i\sigma t + ikx + ily}$, then (8) implies that

$$-k^2 - l^2 - \frac{\beta k}{\sigma} + \frac{\sigma^2 - f_0^2}{gD} = 0. \tag{9}$$

This relation between k, l and σ is more useful when rewritten as

$$\left(k - \frac{\beta}{2\sigma}\right)^2 + l^2 = \left(\frac{\beta}{2\sigma}\right)^2 + \frac{\sigma^2 - f_0^2}{gD}. \tag{10}$$

We see from this equation that high and low frequency waves have significantly different character in the $k - l$ plane. High frequency waves, correspond to $\beta = 0$ which give circles centered at the origin with wavelength $\left(\left(\sigma^2 - f_0^2\right)/gD\right)^{1/2}$. These correspond to gravity modes which are characterized by $\sigma > f$ and are discussed in Section 3. For low frequencies, we have circles centered at $k = \beta/2\sigma$, $l = 0$ with radius less than $\beta/2\sigma$ so that the circles are entirely in the $k > 0$ plane. These are known as Rossby modes and are discussed in Section 4.

A third type of free wave is due to the influence of rotation. These "Kelvin" waves move along the direction of the physical boundary, e.g. the coast of a continent, and decay in magnitude as the distance from the boundary increases. For large enough basins, sum of the normal modes consist of an integral number of Kelvin waves around the boundary. An example of this will be seen in the discussion of gravity waves in a circular basin in Section 3.

3 Gravity Modes

It is instructive to solve the LTE in the context of some very simplified cases first, because the resulting motions are simplified illustrations of the true dynamics. If there is no rotation ($f = 0$), the LTE are given by

$$u_t = -g\zeta_x, \tag{11}$$

$$v_t = -g\zeta_y, \tag{12}$$

$$\zeta_t + D_0(u_x + v_y) = 0, \tag{13}$$

with the boundary condition that

$$\mathbf{u} \cdot \hat{\mathbf{n}} = 0 \tag{14}$$

at the coast, where $\hat{\mathbf{n}}$ is the unit vector normal to the coast. Substituting (11)-(12) into (13), we attain a Helmholtz equation:

$$\nabla^2 \zeta + (\sigma^2/gD)\zeta = 0, \tag{15}$$

with

$$\vec{\nabla}\zeta \cdot \hat{\mathbf{n}} = 0 \tag{16}$$

at the coast.

3.1 Square Basin

We first consider a rectangular basin (Fig. 1) with $A > B$. A general solution can be found by substituting

$$\zeta_{nm} = e^{-i\sigma_{nm}t} \cos\left(\frac{n\pi x}{A}\right) \cos\left(\frac{m\pi y}{B}\right) \tag{17}$$

into (15), which gives the dispersion relation

$$\sigma_{nm}^2 = gD_0 \left[\left(\frac{n\pi}{A}\right)^2 + \left(\frac{m\pi}{B}\right)^2\right]. \tag{18}$$

The gravest mode is then given by

$$T_{10} = \frac{2A}{\sqrt{gD_0}}, \tag{19}$$

where A is the length of the longer side. For all subsequent modes of oscillation,

$$T_{mn} > \frac{2A}{\sqrt{gD_0}}. \tag{20}$$

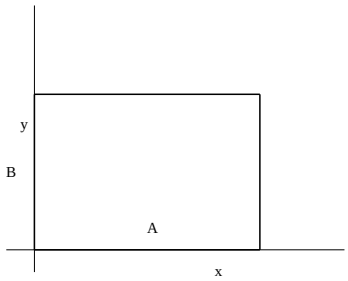

Figure 1: Rectangular ocean basin.

3.2 Circular Basin

In the real world, of course, ocean basins are not rectangular. The next general case that we can consider is that of a circular basin (figure 2). In this case, it is helpful to transform (15) to polar coordinates:

$$\zeta_{rr} + \frac{\zeta_r}{r} + \frac{\zeta_{\phi\phi}}{r^2} + \frac{\sigma^2}{gD_0}\zeta = 0, \tag{21}$$

with boundary condition

$$\zeta_r|_{r=a} = 0. \tag{22}$$

The general solution, which can be derived using separation of variables, is then given by

$$\zeta_{ns} = J_s(\kappa_{ns} r) e^{-i\sigma_{ns}t + is\phi}. \tag{23}$$

The appropriate eigenvalues for the κ_{ns} are determined by the boundary condition; that is

$$J_s'(\kappa_{ns}a) = 0. \tag{24}$$

Finally, the dispersion relation, obtained by plugging (23) into (21), is

$$\sigma_{ns}^2 = gD_0\kappa_{ns}^2. \tag{25}$$

This dispersion relation produces an ascending sequence of eigenfrequencies, σ_{ns}^2.

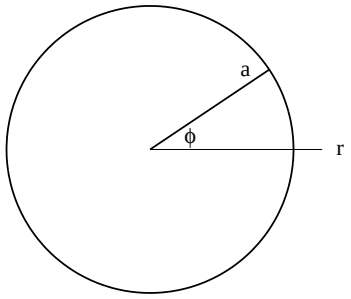

Figure 2: Circular ocean basin.

3.3 Circular Basin with Rotation

We can now add rotation to the problem in a simple way, but setting the Coriolis parameter $f = f_0$. For simplicity, we will keep the depth constant ($D = D_0$). The tidal equations are now given by

$$\begin{aligned} u_t - f_0 v &= -g\zeta_x, & (26)\\ v_t + f_0 u &= -g\zeta_y, & (27)\\ \zeta_t + D_0(u_x + v_y) &= 0, & (28) \end{aligned}$$

with the boundary condition, as before, given by (14). The Helmholtz equation can then be similarly derived, and is given by

$$\nabla^2\zeta + (\frac{\sigma^2 - f_0^2}{gD_0})\zeta = 0, \tag{29}$$

with the boundary condition

$$-i\sigma\zeta_n - f_0\zeta_s = 0 \tag{30}$$

at the coast.

Separable solutions now occur only in a circular basin. In polar coordinates, the Helmholtz equation with rotation is given by

$$\zeta_{rr} + \frac{\zeta_r}{r} + \frac{\zeta_{\phi\phi}}{r^2} + \frac{\sigma^2 - f_0^2}{gD_0}\zeta = 0, \tag{31}$$

with boundary condition

$$-i\sigma\zeta_r - \frac{f_0\zeta_\phi}{a} = 0. \tag{32}$$

The general solution is again given by (23), but now with a modified dispersion relation,

$$\sigma_{ns}^2 = f_0^2 + gD_0\kappa_{ns}^2. \tag{33}$$

For $s = 0$ (that is, no wave in the radial direction), the solution, boundary condition, and dispersion relation are given by

$$\begin{aligned} \zeta_{n0} &= J_0(\kappa_{n0}r)e^{-i\sigma_{0n}t}, & (34)\\ J_0'(\kappa_{n0}a) &= 0, & (35)\\ \sigma_{n0}^2 &= gD_0\kappa_{n0}^2. & (36) \end{aligned}$$

The boundary condition given by (35) again fixes κ_{n0}, with an ascending sequence of positive eigenfrequencies following. This case is just like the case of no rotation ($f_0 = 0$), except that particle paths will now no longer be radial. For $s \neq 0$, substituting the dispersion relation given by (33) into (32) gives

$$-i\sigma\kappa_{ns}J_s'(\kappa_{ns}a) = \frac{f_0 is}{a}J_s(\kappa_{ns}a) = 0, \tag{37}$$

which fixes κ_{ns}. Solving (37) for σ and substituting (33), we have

$$\frac{sJ_s(\kappa a)}{\kappa a J_s'(\kappa a)} = \pm\sqrt{1 + \frac{(\kappa a)^2}{\beta}}, \tag{38}$$

where

$$\beta := \frac{f_0^2 a^2}{gD_0} \tag{39}$$

is called the Lamb Parameter.

Solutions admitted by this problem are given by the roots of (38), as illustrated in figure 4. For a given s, and $f_0 \to 0$ (and, consequently, $\beta \to 0$) the roots are given by $(\kappa a)^2 > 0$ pairs near the $J_s'(\kappa a) = 0$ line. As f_0 and β increase, $(\kappa a)^2$ pairs move farther apart, and a new root appears, with $(\kappa a)^2 < 0$. For this case, κ, and therefore the argument of the Bessel function in (23) will be an imaginary number. The radial part of the solution is then given by a modified Bessel function,

$$I_s(\kappa r) = i^{-n}J_n(ix) = e^{-n\pi i/2}J_n(xe^{i\pi/2}), \tag{40}$$

which decays away from the boundary. Figure 3 shows the dispersion relation given in (33) for a fixed s and different n. The pairs of eigenfrequencies corresponding to the κa pairs in figure 4 can be readily seen; they are gravity waves propagating in opposite directions. The $(\kappa a)^2 < 0$ mode is the Kelvin Wave.

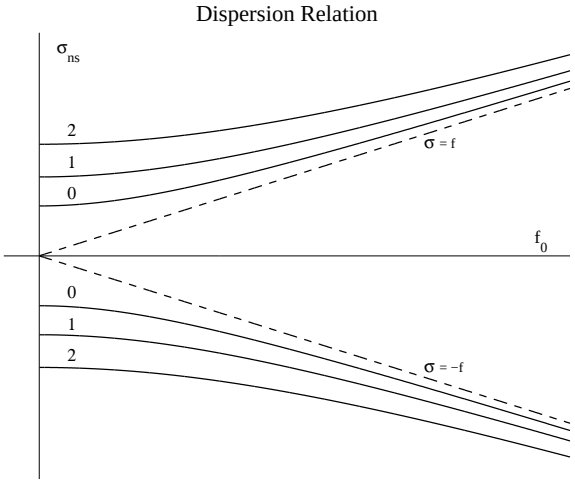

Figure 3: The dispersion relation (33) for different values of n. The Kelvin modes are shown by the dashed line.

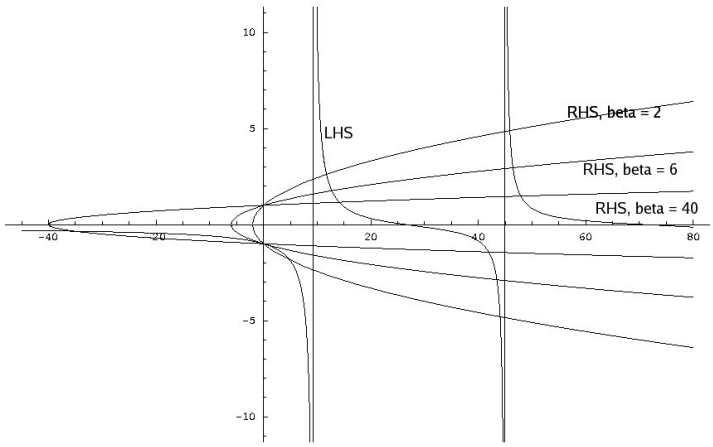

Figure 4: Illustration of the roots of (38). The curves opening to the right correspond to the right hand side of (38) for different β (with β increasing for tighter curves. The asymptotic function is the left hand side of (38). For this case, $s = 2$.

4 Rossby Modes

4.1 Linear Models for Rossby Waves

We now return to the Rossby modes. As discussed earlier, these are the low frequency solutions of the LTE in plane coordinates. Now defining the vorticity, ξ, in the usual way, i.e.

$$\xi = v_x - u_y, \tag{41}$$

we rewrite the shallow water wave equations to give

$$\frac{D}{Dt}\left(\frac{\xi + f}{D}\right) = 0, \tag{42}$$

where D/Dt is the material derivative, i.e.

$$\frac{D}{Dt} = \frac{\partial}{\partial t} + u\frac{\partial}{\partial x} + v\frac{\partial}{\partial y}.$$

Recalling that $f = f_0 + \beta y$ and $D = D_0 + \zeta$ we linearize (42) with respect to ξ, ζ, u and v to find an equation for the time evolution of the vorticity.

$$\begin{aligned}\frac{D}{Dt}\left(\frac{\xi + f}{D}\right) &= \frac{D}{Dt}\left(\frac{\xi + f_0 + \beta y}{D_0} - \frac{(f_0 + \beta y)\,\zeta}{D_0^2}\right) \\ &= \frac{\xi_t}{D_0} - \frac{f_0\zeta_t}{D_0^2} + \frac{\beta v}{D_0},\end{aligned} \tag{43}$$

where we have assumed that $\beta y \ll f_0$ to neglect the term proportional to $\beta y\zeta$.

Since Rossby waves are low frequency waves, $u_t \ll f_0 v$ and $v_t \ll f_0 u$ so that

$$-f_0 v \approx -g\zeta_x \quad f_0 u \approx -g\zeta_y. \tag{44}$$

Substituting (44) into (43), we find that we can rewrite (43)

$$\frac{g}{f_0 D_0}\left(\zeta_{xx} + \zeta_{yy}\right) - \frac{f_0}{D_0^2}\zeta_t + \frac{\beta g}{f_0 D_0}\zeta_x = 0. \tag{45}$$

Multiplying (45) through by $f_0 D_0/g$ (45) becomes

$$\nabla^2\zeta_t - \left(\frac{f_0^2}{gD_0}\right)\zeta_t + \beta\zeta_x = 0. \tag{46}$$

By considering the boundary condition on the coast, we can further simplify the vorticity equation for Rossby waves. As in the earlier discussion of gravity waves, at the coast we must have

$$\mathbf{u}\cdot\hat{\mathbf{n}} = 0,$$

so that if we define a local coordinate system at each point on the coast with the $\hat{\mathbf{s}}$ direction tangent to the coast, we must have $\zeta_s = 0$ so that

$$\zeta_{coast} = \Gamma(t), \tag{47}$$

i.e. that value of ζ is the same everywhere on the coast though it may be allowed to vary in time. For sufficiently short waves,

$$\nabla^2 \zeta_t \gg \left(\frac{f_0^2}{g D_0} \zeta_t \right), \tag{48}$$

so that to leading order (46) becomes

$$\nabla^2 \zeta_t + \beta \zeta_x = 0. \tag{49}$$

Since the boundary condition is independent of space, the time dependent boundary condition can, to leading order, be absorbed into ζ, so that (49) can be solved under the condition

$$\zeta_{coast} = 0. \tag{50}$$

4.2 Rossby Waves in a Square Basin

Suppose that ζ is periodic in time with frequency σ. That is, suppose that ζ can be written in the form

$$\zeta(x, y, t) = \Re \left\{ e^{-i\sigma t} \Phi(x, y) \right\}. \tag{51}$$

Substituting this expression for ζ into (49), we find that Φ satisfies the following boundary value problem.

$$\nabla^2 \Phi + \frac{i\beta}{\sigma} \frac{\partial \Phi}{\partial x} = 0, \quad \Phi_{coast} = 0. \tag{52}$$

To remove the x-derivative from (52) we further substitute

$$\Phi = e^{-i\beta x / 2\sigma} \phi(x, y) \tag{53}$$

into equation 52 we find that ϕ satisfies the boundary value problem

$$\nabla^2 \phi + \lambda^2 \phi = 0, \phi_{coast} = 0, \tag{54}$$

where $\lambda^2 = \beta^2 / 4\sigma^2$.

Consider Rossby waves in the rectangular basin $0 \leq x \leq x_0$, $0 \leq y \leq y_0$. Using separation of variables, we write

$$\phi(x, y) = X(x) Y(y) \tag{55}$$

and see that X and Y both satisfy equations for the harmonic oscillator. Therefore the boundary conditions imply that any function of the form

$$\phi = \phi_{mn} = \sin \frac{m\pi x}{x_0} \sin \frac{n\pi y}{y_0}, \tag{56}$$

with m, n positive integers, satisfies the boundary value problem and that σ is the corresponding eigenvalue,

$$\sigma = \sigma_{mn} = -\frac{\beta}{2\pi} \frac{1}{\left[\left(m^2 / x_0^2 \right) + \left(n^2 / y_0^2 \right) \right]^{1/2}}. \tag{57}$$

Note that the highest frequency modes are the ones with the smallest values of m and n. Substituting, our solution for ϕ_{nn} into (53) and subsequently into (51), we find that for each normal mode

$$\zeta = \cos\left[\frac{\beta x}{2\sigma_{mn}} + \sigma_{mn} t\right] \sin\left(m\pi \frac{x}{x_0}\right) \sin\left(n\pi \frac{y}{y_0}\right). \tag{58}$$

This solution consists of a carrier wave moving to the left modulated by sine function serving to satisfy the boundary conditions. The sine functions also create stationary nodes while the cosine function creates nodes which move to the left.

4.3 Circular Basin

Now suppose we have a circular basin with radius a. The definitions for ϕ follow exactly the same as for the square basin leaving the boundary value problem

$$\nabla^2 \phi + \lambda^2 \phi = 0, \quad \phi\,(r = a) = 0, \tag{59}$$

with $\lambda^2 = \beta^2/4\sigma^2$.

We again use separation of variables to write

$$\phi = R\,(r)\,\Theta\,(\theta) \tag{60}$$

to find that Θ and R satisfy the harmonic oscillator and Bessel Equations respectively. Therefore, the boundary conditions and single-valuedness imply that any function of the form

$$\phi = \phi_{nm} = \cos\,(m\theta + \alpha)\, J_m\,(k_{nm} r)\,, \tag{61}$$

with α an arbitrary phase angle, satisfies the boundary conditions under the conditions that m is a positive integer, J_m is the Bessel Function of order m, and

$$\xi_{mn} = k_{nm} a \tag{62}$$

is the n^{th} zero of the Bessel function of order m. The eigenvalue for σ is then

$$\sigma_{mn} = -\frac{\beta}{k_{nm}^2 a^2}, \tag{63}$$

and the corresponding eigenfunction is

$$\zeta_{mn} = \cos\left[\frac{\beta x}{2\sigma_{mn}} + \sigma_{mn} t\right] \cos\,(m\theta + \alpha)\, J_m\,(k_{nm} r)\,. \tag{64}$$

Therefore these eigenfunctions also represent a carrier wave moving to the left creating moving nodes modulated by an envelope of functions which create stationary nodes. In this case the stationary modes are radial lines corresponding to zeros of $\cos\,(m\theta + \alpha)$ and circles corresponding to zeros of $J_m\,(k_{nm} r)$.

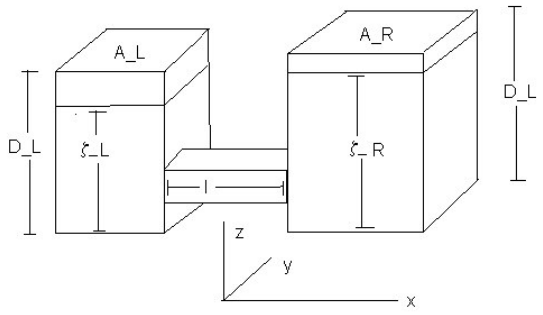

Figure 5: The Helmholtz Oscillator

5 Helmholz "Mass Exchange" Mode

We can solve for an additional normal mode, where fluid moves between two basins. The problem is illustrated in Fig. 5 in which A_L, D_L and A_R, D_R represent the cross-sectional area and depth of the left and right basins respectively. We further take l, w, and d to be the length, width, and depth of the connecting channel.

If we take $D_L, D_R \gg d$ so that the fluid height, ζ, in each basin can be taken as virtually constant within the basin and the connecting channel is always full. Define ζ_L and ζ_R as the time dependent fluid heights in the left and right basins, respectively. The total fluid volume in the system is

$$V = A_L\zeta_L + A_R\zeta_R + lwd \tag{65}$$

and must be conserved conserved. Differentiating (65) with respect to time, we derive the volume conservation equation:

$$A_L\left(\zeta_L\right)_t + A_R\left(\zeta_R\right)_t = 0. \tag{66}$$

Since we have taken ζ_L and ζ_R to be independent of space, we can express the time rate of change of the volume flux into the right basin as

$$\frac{d}{dt}A_R\left(\zeta_R\right)_t = A_R\left(\zeta_R\right)_{tt}.$$

Any fluid that enters the right basin must enter through the connecting channel. If we assume the velocity of the fluid in the channel is entirely in the lengthwise direction, then the fluid flux into the right basin is uwd, where u is the fluid velocity in the lengthwise direction and taken to be parallel to the x-axis. Therefore, equating the time rate of change of fluid into the right basin gives us

$$A_R\left(\zeta_R\right)_{tt} = u_t wd. \tag{67}$$

Since we have assumed that the flow in the channel is uniform and unidirectional, the momentum equation in the channel is $u_t = -g\zeta_x$. At the left edge of the channel, $\zeta = \zeta_L$

while $\zeta = \zeta_R$ at the right edge. Therefore, since the length of the channel is l, $\zeta_x \approx (\zeta_R - \zeta_L)/l$. Therefore, we can rewrite (67) as

$$A_R (\zeta_R)_t \, t \approx -wdg \frac{\zeta_R - \zeta_L}{l}. \tag{68}$$

Solving (65) for ζ_L and substituting into (68) we find that ζ_R satisfies the equation for a simple harmonic oscillator. That is

$$(\zeta_R)_{tt} + gwd \left(\frac{1}{A_R} + \frac{1}{A_L} \right) \zeta_R = K, \tag{69}$$

where K is a constant. This equation implies that the Helmholtz mass exchange mode does represent a simple wave solution of the shallow water wave equations with

$$\omega^2_{Helmholtz} = gwd \left(\frac{1}{A_R} + \frac{1}{A_L} \right). \tag{70}$$

6 Platzman's Analysis

Platzman et al. [1] computed approximate normal modes of the world oceans by computing the normal modes in the 8 to 80-hour spectrum of a numerical model of the LTE. Platzman's analysis focuses on large-scale features of the direct response of the deep ocean to the tidal potential, rather than coastal tides. The discretization of the model makes it an eigenvalue problem with 2042 total degrees of freedom. The eigenvectors have the form

$$(\xi, \phi, \psi) = Re[(Z, \Phi, \Psi) e^{i\sigma t}], \tag{71}$$

where σ is the eigenfrequency, ξ is the free surface elevation, ϕ is velocity potential, and ψ is the volume streamfunction.

Platzman et al. visualized the different normal mode motions described in the previous sections, by contouring the amplitude and phase of the mean elevation, as well as the energy density and flux, over the model grid. It is instructive to examine some example maps, which illustrate different normal modes.

Figure 6 shows a sample analysis from Platzman et al., of a topographic vorticity wave, as contained by the 14th computed normal mode, which has a period of $T = 33h$. The height contour plot in this figure (left panel) shows a sort of height "dome", and the phase lines (perpendicular to the lines of height) show the counterclockwise rotation about an amphidrome where the phase contours are anchored. The energy diagram (right panel) shows that energy is transported in an anticyclonic gyre, with the energy flow largely parallel to the phase velocity of the wave. (Since the study only looked for modes with periods between 8 and 80 hours, it couldn't clearly resolve any planetary vorticity waves.)

Similarly, Mode 12 (Fig. 7) can be understood, given the height and energy contours as the Helmholtz resonator mode described in section 5. The energy diagram for this mode shows a nearly uniform phase across each ocean, and the elevation contours could perhaps be interpreted as having a "node-like band" at the junction between the two oceans. A clearer argument for the Helmholtz resonator analogy is given by Fig. 8, which simply

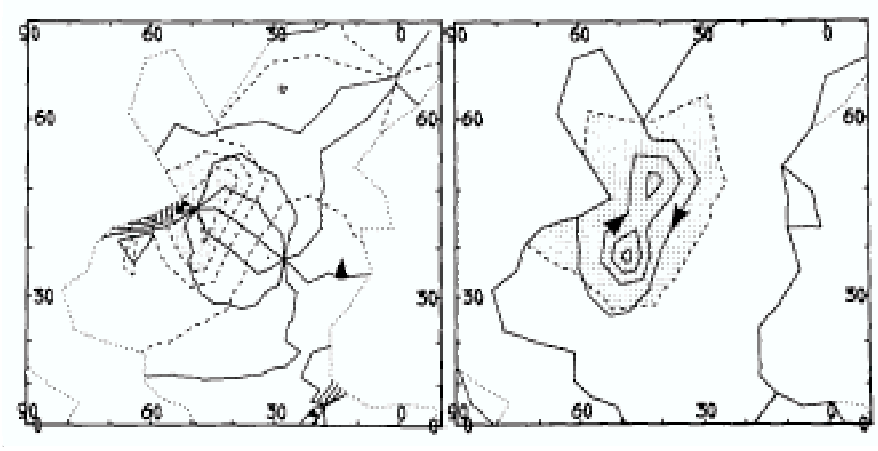

Figure 6: Platzman et al.'s computed mode 14, a vorticity wave near Newfoundland. Elevation is contoured in the left panel, total energy density on the right. Arrows are placed on the contour of zero phase, and point in the direction of phase propagation.

shows a polar plot of the amplitude and phase of the fluctuations in regional volume which are induced by that particular mode.

This figure suggests that the volume of the Arctic and North Atlantic oceans are in balance with the Indian and South Atlantic Oceans.

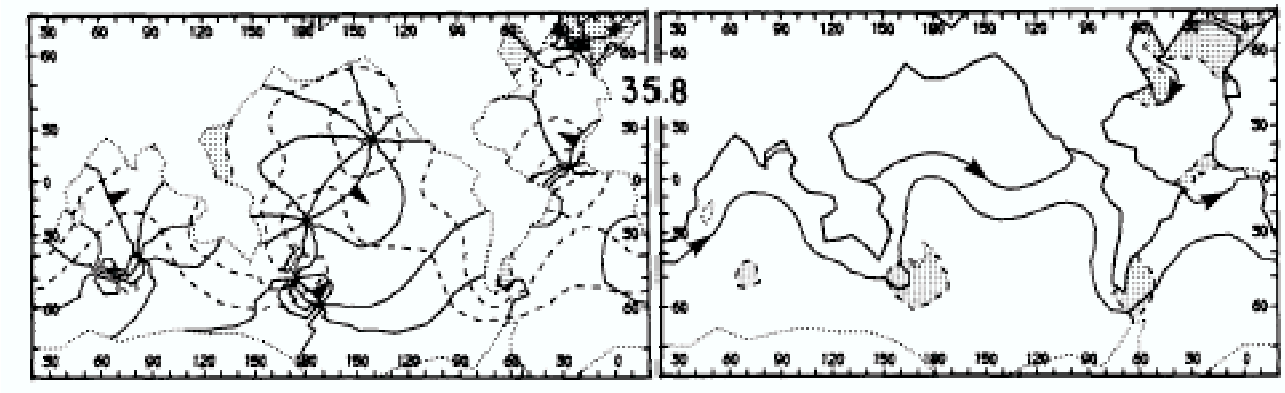

Figure 7: Platzman et al.'s computed mode 12, which can be interpreted as a Helmholtz resonator mode.

Mode 12 carries less than 30% rotational kinetic energy. Mode 15 (Fig. 9) also carries little rotational energy, though it also has a clear Kelvin Wave component in the southern ocean, with phase lines parallel to the coast of Antarctica, and eastward energy propagation.

As for gravity modes (Section 3), Platzman et al.'s model resolves 5 slow ($T < 24h$) gravity modes, but these tend to take on the appearance of vortical modes in the presence

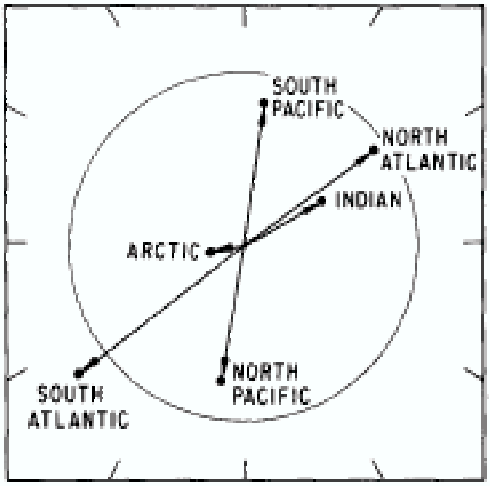

Figure 8: Volume-fluctuation vectors for Platzman et al.'s mode 12.

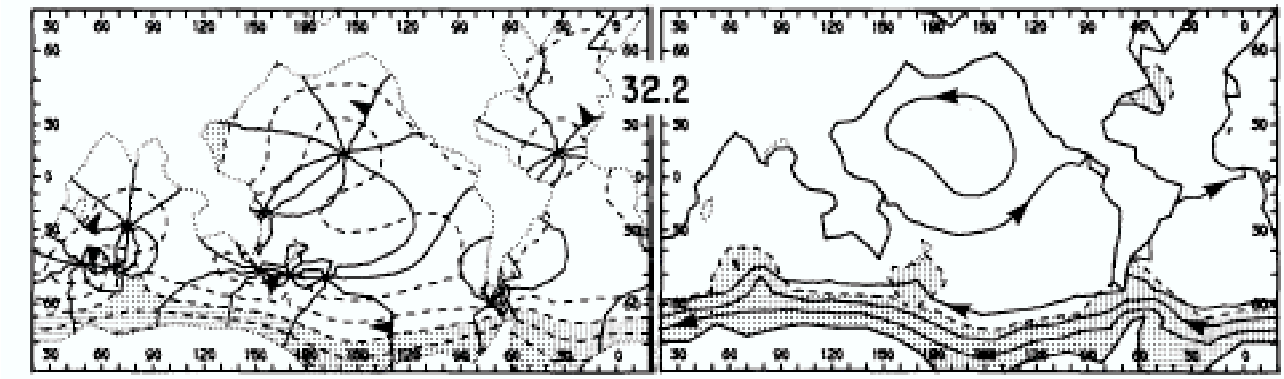

Figure 9: Platzman et al.'s computed mode 15, which contains a Kelvin Wave component.

of bottom topography. An example of a fast gravity wave is shown in figure 10, of mode 28. In this example, the arctic ocean seems to be strongly excited, and the arctic energy density is much larger than the global average.

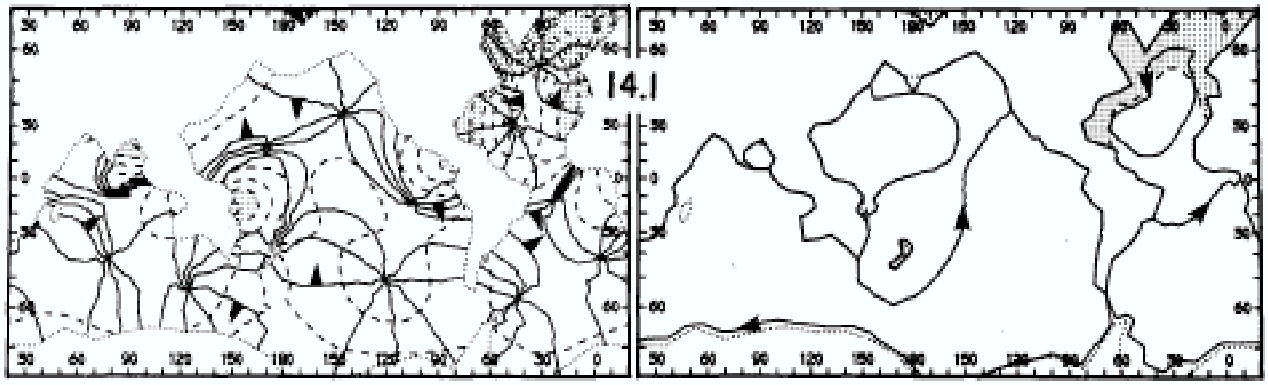

Figure 10: Platzman et al.'s computed mode 28, a gravity wave.

7 Resonance

The response of the oceans to tidal forcing at frequency ω, given a spectrum of ocean normal modes, can be written as

$$\zeta(\mathbf{x},t) = \mathbf{Re}\sum_n \frac{B_n(\omega)}{\omega_n - \omega - \frac{1}{2}iQ_n^{-1}\omega_n} S_n(\mathbf{x})e^{-i\omega t}, \tag{72}$$

where ω_n is the frequency of the nth normal mode of the oceans, $S_n(\mathbf{x})$ is the corresponding eigenfunction, and $B_n(\omega)$ is a complex factor that needs to be somehow determined. Q_n is a dissipation factor; that is, the nth normal mode dissipates a fraction $2\pi Q_n^{-1}$ of its energy per cycle. The response function given in equation (72) assumes that the functions $S_n(\mathbf{x})$ form a complete set. Equation (72) also makes the implicit assumption that the normal modes are linear waves. This assumption does not really hold in shallow water, where the nonlinear friction terms become significant. It is instructive to examine equation (72) for a hypothetical case where one mode (say,the zeroth mode) dominates, and its corresponding spatial response is constant, such that $B_0(\omega)S_0(\mathbf{x}) = C_0$. Then we can write

$$Ae^{i\Theta} = \frac{C_0}{\omega_0 - \omega - \frac{1}{2}iQ^{-1}\omega_0}. \tag{73}$$

This response function is plotted in figure 11. The age of the tide (i.e. the time lag between the tidal potential and the maximum of the response) can be found from $d\Theta/d\omega$, which, in this simple case, is given by

$$\frac{d\Theta}{d\omega} = \frac{\frac{1}{2}Q_0^{-1}\omega_0}{(\omega_0 - \omega)^2 + (\frac{1}{2}Q_0^{-1}\omega_0)^2}. \tag{74}$$

For the single-mode case, the maximum value is $2Q_0/\omega_0$ (at $\omega = \omega_0$). If the tide were dominated by single ocean mode, the age of the tide would be positive, and the same everywhere. Since

$$Q_0 \geq \frac{1}{2}\omega_0 \frac{d\Theta}{d\omega} \tag{75}$$

the age of the tide would put a lower limit on the quality factor Q_0.

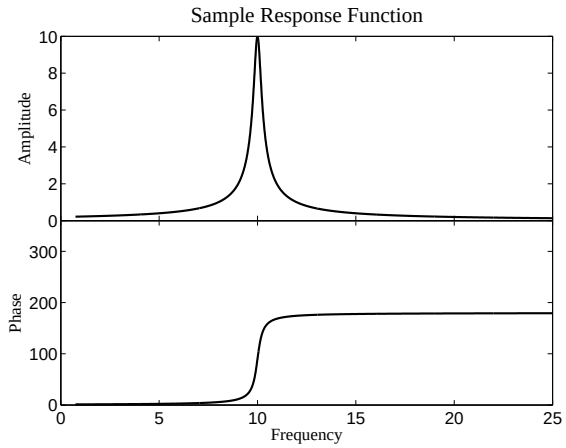

Figure 11: Sample response function for a single normal mode, where we have chosen $w_0 = 1$, $Q_0 = 25$, and $C_0 = 1$.

8 Comments on Inferences drawn from Ocean Models

Looking at the models for the ocean's normal modes we have just discussed, we can draw some interesting conclusions. Taking the dynamical solution of the "time scale" problem for the lunar orbit evolution as being solved by Hansen [2], Webb [3], Ooe et al. [4], and Kagan and Maslova [5], the models generate significantly smaller torques in the past than that implied by earth's present rotation rate. Platzman's work explains that the ocean has many different normal modes, some of which have frequencies close to the main tidal spectral lines. The modes grow more complex as frequency increases. In the past, the Earth's faster rotation forced tidal frequencies higher so that the modes with near-tidal frequencies were less well matched spatially to the large-scale tidal forcing, so that they were less easily excited. Therefore the torques were smaller since the tidal admittance to the tidal potential was also decreased from its current day value.

9 Why Ocean Tides are Back in Fashion

The LTE were written down 1776, so why are we still studying tides in 2004? There are several reasons: understanding why certain places see such large tides, understanding tidal dissipation from internal tide mixing, and the possibility of using the tides as a renewable energy source. We will discuss the first of these in this lecture.

Name	Type	Period(h)	Amp.
Q_1	L	26.87	0.0641
O_1	L	25.82	0.3800
P_1	S	24.07	0.2011
K_1	L/S	23.93	0.6392
N_2	L	12.66	0.0880
M_2	L	12.42	0.3774
S_2	S	12.00	0.1089

Table 1: Dominant constituents at Victora

10 The Tides at Victoria

If the moon were perfectly aligned with the equator, its motion would only cause semi diurnal tides. However, the moon orbits the earth at a declination angle which means that it also forces a diurnal tide. The dominant semi diurnal and diurnal tides at Victoria, BC, can be seen in Table 1.

The interactions of these tides account for the daily variations in the tides. M_2 and S_2 beat over the spring/neap cycle. K_1 and O_1 beat over a lunar month to allow for changes in the moon's declination which modulates the lunar diurnal tide. K_1 and P_1 beat over a year to allow for changes in the sun's declination which accounts for changes in the solar diurnal tide. Furthermore, M_2 and N_2 beat to provide a correction allowing for ellipticity in the moon's orbit which also effects the lunar diurnal tide.

Since K_1 has the largest amplitude we expect the tides in Victoria to look mostly diurnal. That is there should be approximately one maximum and one minimum tide during the day with some variations due to the other tides. However, in the third week of March 2004, for example, there were several consecutive days where there are two distinct maxima and minima. This is an example of the beating discussed in the previous paragraph. At the spring perigee, the sun and the moon were very close to the equatorial plane which diminishes the diurnals allowing the semidiurnals to appear more prominently, particularly at spring tides.

11 The World's Highest Tides

Two Canadian locations have recently both claimed that they have the world's largest tides. In the upper part of the Bay of Fundy, the tides rise up to 17m. Ungava Bay in Quebec also has tides that can reach at least 16.8m. Both of these maxima occur in an 18.61 year nodal cycle.

There have been several "explanations" offered by various sources for why the tides in the Bay of Fundy are so large. These include the idea that the Bay of Fundy is the closest point to the moon at these times and the belief that large tidal currents from the Indian Ocean can enter the bay because it opens to the south! In actuality, these large tides are more likely connected to a resonance phenomenon [6], which will be discussed in the next section.

12 Friction and Resonance

The time lag between the spring/neap cycles of the different tidal potential constituents, and the actual observed response of the oceans, is called the age of the tide [7]. It can be explained mathematically in terms of the response function given in (72) introduced in Section 7. The effect of friction can be examined more closely by approximating the energy dissipated due to friction, which is proportional to $u|u|$. If we assume that the tidal current u is the sum of a primary tidal constituent and a secondary, weaker one,

$$u = u_0(\cos\omega_1 t + \epsilon\cos\omega_2 t), \tag{76}$$

(where ϵ is a small parameter) then it can be shown that

$$u|u| = \frac{8}{3\pi}u_0^2(\cos\omega_1 t + \frac{3}{2}\cos\omega_2 t + ...), \tag{77}$$

where we have neglected higher-order harmonics. The 3/2 coefficient in the second term of (77) shows that the weaker tide feels a stronger frictional effect. In other words, the Q factor for the weaker tide will be 2/3 that of the stronger tide.

The response of the Bay of Fundy and the Gulf of Maine implies a resonant period of about 13.3 hours and a Q, for M_2, of about 5. On the west coast, the tidal response of the Strait of Georgia and Puget Sound can be modeled as a Helmholtz Resonance, where the tidal current enters a bay of surface area A through a channel of length L and cross section E. We will assume that the bay is small enough such that the height of the water surface rises uniformly everywhere. If the tide outside the bay is $a\cos\omega t$, the level inside is $\mathbf{Re}(a'e^{-i\omega t})$, where a' is the response amplitude in the bay. The current in the entrance channel is $\mathbf{Re}(ue^{-i\omega t})$. The continuity equation is is then

$$-i\omega a'A = Eu. \tag{78}$$

The channel dynamics are a balance between acceleration, friction, and the pressure gradient. The momentum equation can be written as

$$-i\omega u + g(a' - a)/L = -\lambda u, \tag{79}$$

where λ is simply a linear damping factor. As shown in equation (77), λ will be 50% larger for the constituents with weaker currents than the dominant M_2. The response in the bay will then be given by

$$a' = \frac{a}{1 - \frac{w^2}{w_0^2} - \frac{i\omega\lambda}{w_0^2}}, \tag{80}$$

where $\omega_0 = (\frac{gE}{AL})^{1/2}$ is the resonant frequency.

The frequency dependent response curve for a Helmholtz resonator given in equation (80). The response for a rectangular bay (not shown) can also be fitted to the data, that is, the tidal constituent frequencies and the corresponding amplitude and phase lag measurements.

For both cases, it seems that the observed tides straddle a resonant frequency ω_0, with $Q = \omega_0/\lambda$. For both cases, the fit returns a $Q \simeq 2$, which is low (and thus corresponds to high friction). This seems to be consistent with the high friction required by numerical models.

13 Nodal Modulation

The effect of the nodal modulation of the tide (due to the variation of the moon's declination) can be similarly written as a response curve, proportional to

$$a \propto \frac{a_0(1+\epsilon)}{1-\frac{\omega}{\omega_0}+\frac{1}{2}iQ_0^{-1}\frac{a}{a_0}}, \tag{81}$$

where the $1+\epsilon$ factor includes the effect of the modulation of semidiurnal forcing and the multiplier in the friction term allows for quadratic friction [8].

Away from resonance, the friction term becomes insignificant, and $a \propto 1+\epsilon$. Near resonance, however, the friction term becomes important, and $a \propto 1+\frac{1}{2}\epsilon$. Indeed, the actual modulation in the Bay of Fundy is less than in other areas.

Notes by David Vener and Lisa Neef

References

[1] G. Platzman, G. Curtis, K. Hansen, and R. Slater, "Normal modes of the world ocean. part ii: Description of modes in the period range 8 to 80 hours," J. Phys. Ocean. **11**, 579 (1981).

[2] K. Hansen, "Secular effects of oceanic tidal dissipation on the moon's orbit and the earth's rotation," Review of Geophysics **20**, 457 (1982).

[3] D. Webb, "Tides and the evolution of the earth moon system," Geophys. J. Roy. Astr. Soc. **70**, 261 (1982).

[4] H. S. M. Ooe and H. Kinoshita, "Effects of the tidal dissipation on the moon's orbit and the earth's ratation," Geophysical Monograph **59**, 51 (1990).

[5] B. Kagan and N. Maslova, "A stochastic model of the earth-moon tidal evolution accounting for the cyclic variations of resonant properties of the ocean: An asymptotic solution," Earth, Moon and Planets **66**, 173 (1994).

[6] C. Garrett, "Tidal resonance in the bay of fundy," Nature **238**, 441 (1972).

[7] C. Garrett and W. Munk, "The age of the tide and the 'Q' of the oceans.," Deep-Sea Res. **18**, 493 (1971).

[8] L. Ku, D. Greenberg, C. Garrett, and F. Dobson, "The nodal modulation of the m_2 tide in the bay of fundy and gulf of maine," Science **230**, 69 (1985).